Materials Chemistry and Physics 333 (2025) 130393

Contents lists available at ScienceDirect

Materials Chemistry and Physics

journal homepage: www.elsevier.com/locate/matchemphys

Atomic structure and properties of amorphous boron carbon nitride (BC_2N): An ab initio study

Murat Durandurdu

Department of Materials Science and Nanotechnology Engineering, Abdullah Gül University, Kayseri, Türkiye

HIGHLIGHTS

- a-BC_2N exhibits a layer-like structure.
- Unlike the ordered arrangement in crystalline BC_2N, a-BC_2N has a random distribution of B, C, and N atoms within each layer.
- a-BC_2N is likely a semiconductor.
- a-BC_2N displays mechanical properties characteristic of layered materials, but with an increased bulk modulus.

GRAPHICAL ABSTRACT

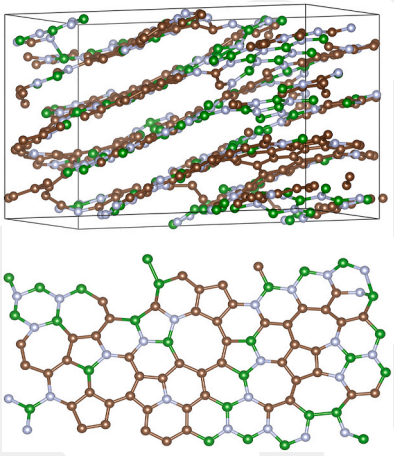

ARTICLE INFO

Keywords:
Amorphous
Boron carbonitride
Graphite-like
ab initio
Energy

ABSTRACT

This study investigates the atomic structure and properties of amorphous boron carbon nitride (a- BC_2N) using ab initio molecular dynamics simulations. Structural analysis reveals a layer-like topology with varied bonding environments. Unlike the ordered alternating C–C and B–N layers found in the lowest-energy crystalline BC_2N structure, a-BC_2N features a solid-solution-like arrangement, with B, C, and N atoms randomly distributed within each layer. This randomness gives rise to small, distinct C-rich and BN-rich domains and irregular short zigzag chains of C–C and B–N bonds within each layer. Electronic structure analysis suggests that a-BC_2N is likely a semiconductor. Mechanically, a-BC_2N displays properties typical of layered materials but with an enhanced bulk modulus.

1. Introduction

Ternary boron carbon nitride (BCN) materials have emerged as a promising class of compounds with potential applications across numerous fields, involving electronics, energy storage, and materials science [1–4]. These materials are notable for their tunable electronic

E-mail address: murat.durandurdu@agu.edu.tr.

https://doi.org/10.1016/j.matchemphys.2025.130393
Received 7 November 2024; Received in revised form 23 December 2024; Accepted 11 January 2025
Available online 11 January 2025

properties and exceptional mechanical strength, especially in diamond-like phases, which has attracted significant attention. Among the diverse BCN compositions, BC_2N stands out due to its unique properties. In particular, the diamond-like phase, d-BC_2N, has been extensively studied [5–19] for its potential to surpass the hardness and chemical stability of both diamond and cubic boron nitride (c-BN). However, determining the precise crystal structure of d-BC_2N remains challenging. The small and similar atomic masses of B, C, and N complicate x-ray diffraction data interpretation, hindering accurate crystallographic characterization. On the theoretical side, multiple potential crystal structures for d-BC_2N [10–20] have been proposed, yet no consensus has been reached.

Hexagonal BC_2N (h-BC_2N) is considered a promising precursor for synthesizing d-BC_2N. Various experimental techniques have successfully produced h-BC_2N in phases that range in structural order, from amorphous and turbostratic to well-ordered configurations [21–29]. Several theoretical researches have focused on understanding the stacking sequences within h-BC_2N [29–36] and a structure with alternating C–C and B–N layers was proposed as the most stable configuration with the lowest total energy among the projected h-BC_2N structures [30].

Conversely, research on amorphous or turbostratic forms of BC_2N is limited, and the properties of amorphous BC_2N (a-BC_2N) remain relatively unexplored. The main purpose of this study is to offer insights into the atomic structure and properties of a-BC_2N. Through comprehensive computational analyses, this study aims to expand understanding of a-BC_2N and explore its potential applications across various fields.

2. Methodology

We employed SIESTA program [37] to model a-BC_2N and investigate its properties of a-BC_2N. Pseudopotentials were due to the Troullier-Martins scheme [38], and calculations utilized double zeta (DZ) basis sets with the Γ-point for Brillouin zone sampling. The Perdew-Burke-Ernzerhof (PBE) generalized gradient approximation (GGA) functional [39] was used with Grimme's dispersion correction [40]. Ab initio molecular dynamics (MD) simulations were achieved in the isothermal–isobaric ensemble (NPT) with a time step of 1.0 fs. In the MD simulations, shear distortion was prohibited, and the supercell was maintained as orthogonal. Temperature control was achieved through velocity scaling, while volume adjustment was maintained using the Parrinello-Rahman approach [41]. The initial configuration was generated by a tetrahedrally coordinated $\bar{p}$ 4m2 crystal structure with unit cell parameters $a = b = 2.56$ Å, c = 3.676 Å and density of 3.3429 g/cm^3, consisting of 384 atoms. This unrelaxed supercell was first exposed to 5000 K for 20.0 ps to simulate melting, then cooled to 4500 K and equilibrized for 50 ps. A gradual quenching process at a rate of 1×10^{13} K/s was employed, with an additional equilibration step at 4000 K for 50 ps before further quenching to 300 K. Final structural relaxation employed the variable cell conjugate gradient method till atomic forces were minimized below 0.01 eV/Å, allowing the atomic positions and simulation cell volume to adjust freely. The density of final amorphous structure is 2.3656 g/cm^3. Partial structural analysis was performed by means of the ISAACS package [42].

3. Results

The atomic configuration of the simulated a-BC_2N material, shown in Fig. 1 using VESTA software [43], reveals a layer-like structure with some atoms bridging between layers. Unlike the ordered C–C and B–N alternating layers of the lowest-energy h-BC_2N, a-BC_2N adopts a solid-solution-like arrangement, where B, C, and N atoms are randomly distributed within each layer. This randomness results in small, distinct C-rich and BN-rich domains, a feature previously discussed in BC_2N systems [1,36]. Furthermore, the disordered arrangement forms irregular short zigzag chains of C–C and B–N bonds, resembling the zigzag configurations characteristic of the most stable BC_2N sheet [35]. The

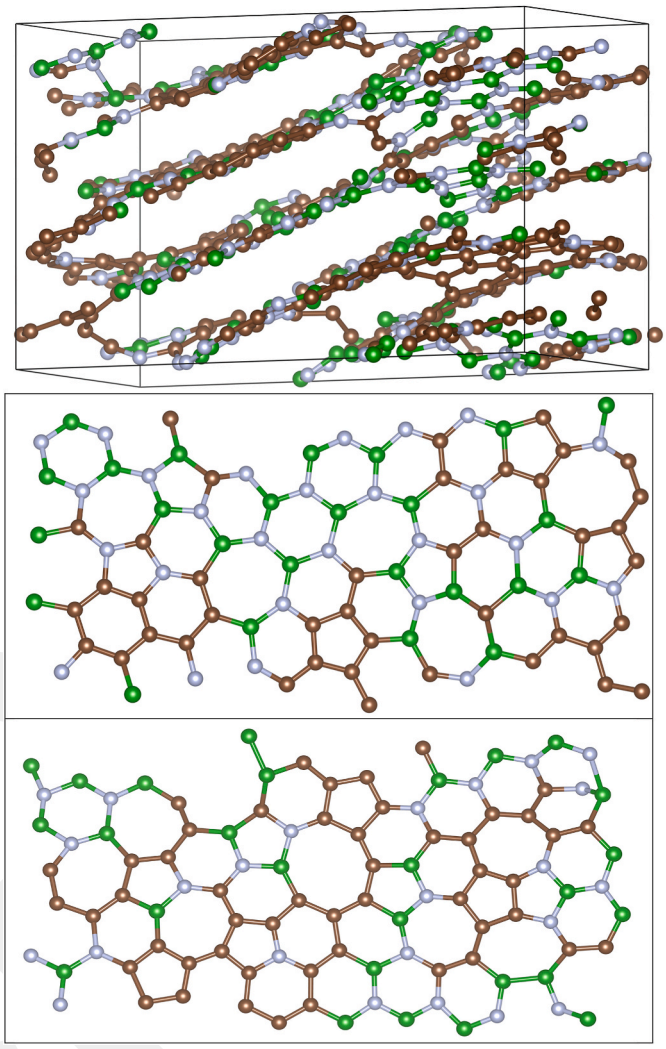

Fig. 1. Atomic configuration of the simulated a-BC_2N material and two distinct layers extracted from the model. Brown, green, and gray colors characterize C, B, and N atoms, correspondingly. (For interpretation of the references to color in this figure legend, the reader is referred to the Web version of this article.)

interlayer spacing in a-BC_2N is manually measured using VESTA program, yielding an average value of approximately 3.07 Å. This spacing is slightly narrower than the 3.31–3.43 Å typically observed in h-BC_2N [24,27,29]. The closer interlayer spacing observed in a-BC_2N may result from the interconnection between layers.

The partial pair distribution function analysis (Fig. 2) offers a detailed view of the local atomic structure in a-BC_2N, capturing bonding interactions among all elements. The mean C–C bond length is found to be 1.42 Å, consistent with the 1.42–1.44 Å bond lengths determined for h-BC_2N [30,31] and amorphous graphite (a-graphite) [44,45]. The average B–N bond distance is detected around 1.45 Å, closely associating with the 1.42–1.45 Å in h-BC_2N [30,31] and the 1.44 Å in BN [46]. The C–N separation is measured at 1.39 Å, within the 1.38–1.51 Å range reported for h- BC_2N [30,31] and the 1.30–1.463 Å range typical of crystalline and amorphous CN [47,48]. The B–C bonds, with a mean length of 1.53 Å, also align well with theoretical values in h-BC_2N (1.37–1.51 Å) [30,31] and BC crystals (1.51–1.55 Å) [49,50]. Notably, the B–B bond in the amorphous phase is shorter, at 1.66 Å, compared to 1.70 Å in h-BC_2N crystals [31].

To further characterize the atomic environments and coordination trends in a-BC_2N, we perform a detailed bonding analysis. Bonding interactions were identified using specific cutoff distances for each atomic

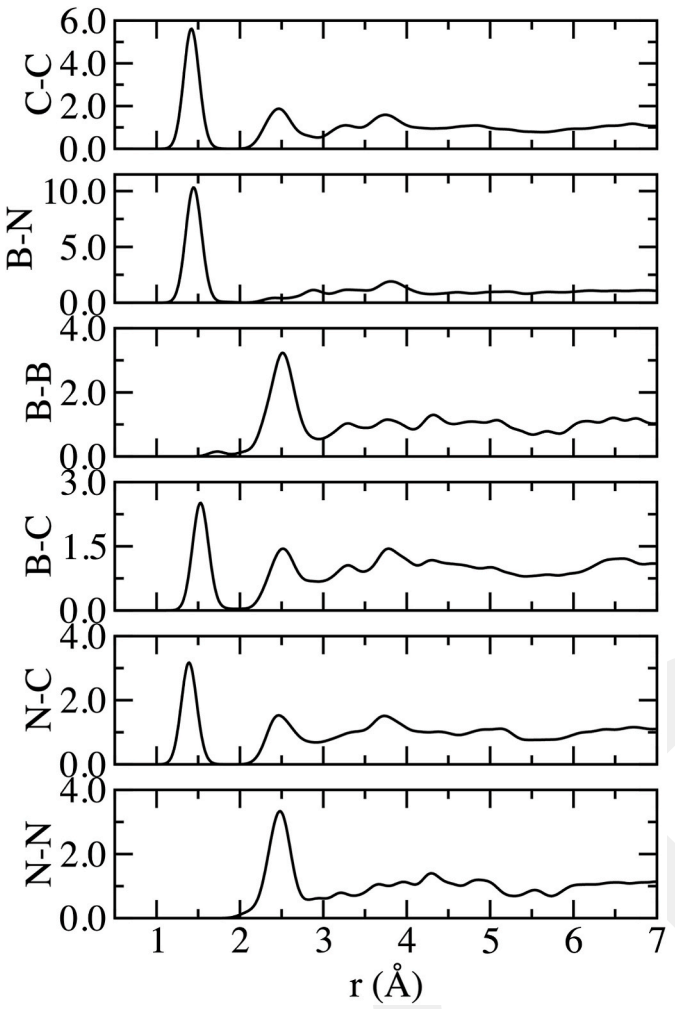

Fig. 2. Partial pair distribution functions (PPDFs) for a-BC_2N, illustrating local structural characteristics.

pair: B–B (1.90 Å), B–C (1.76 Å), C–C (1.86 Å), B–N (1.73 Å), and C–N (1.80 Å). These parameters allowed us to determine coordination numbers and examine elemental bonding patterns within the amorphous network. Most C atoms (~99 %) present threefold coordination, with an insignificant subset forming four bonds, resulting in an average of 3.01, predominantly C–C bonds (1.958). C atoms also participate in bonds with B atoms (C–B: 0.52) and N atoms (C–N: 0.53), showing a significant role for C–B and C–N bonding. B atoms consistently display threefold coordination with an average coordination number of 3.0. They preferentially bond with N (B–N: 1.916) and C (B–C: 1.04), while B–B bonding is minimal (B–B: 0.041). N atoms exhibit 98 % threefold coordination, with 2 % forming two bonds and an average coordination number of 2.97. They predominantly bond with B atoms (N–B: 1.916) and C atoms (N–C: 1.062). Overall, B–N and C–C bonds dominate the bonding environment, with B–C and C–N bonds contributing additional connectivity.

The chemical environment analysis, detailed in Table 1, complements the coordination findings by highlighting the specific bonding configurations most common to each element within the amorphous network. This analysis categorizes the most common bonding arrangements for each element in the amorphous network. For C atoms, the most prevalent configuration is C–C_3, comprising 26.56 % of carbon environments. This is followed by C–C_2N at 25 %, and C–C_2B at 22.4 %. For B atoms, the analysis reveals a dominant presence of B–N_2C at 43.75 %, followed by B–NC_2 and B–N_3, each representing 25 % of B environments. This trend indicates that B atoms favor bonding with N while also

Table 1
Chemical characteristics surrounding each species in a-BC_2N.

C		B		N	
C_3	26.56 %	N_2C	43.75 %	B_2C	38.54 %
C_2N	25.00 %	NC_2	25.00 %	B_3	29.17 %
C_2B	22.40 %	N_3	25.00 %	BC_2	25.00 %
CBN	8.85 %	C_3	2.08 %	C_3	5.21 %
CN_2	6.25 %	NBC	2.08 %	BC	2.08 %
CB_2	5.31 %	N_2B	1.04 %		
B_2N	2.60 %	C_2B	1.04 %		
BN_2	1.56 %				
C_2BN	0.52 %				
B_3	0.52 %				
CB_3	0.52 %				

forming mixed bonds with C. For N atoms, the most common configuration is N–B_2C at 38 %, with N–B_3 at 29 % and N–BC_2 at 25 %.

The bond angle distribution analysis in Fig. 3 reveals a prominent peak around 120°, suggesting a dominant trigonal symmetry within the atomic structure. The network is composed of four-to eight-membered rings, with a predominance of six-membered rings as shown by the ring statistics analysis in Fig. 4. Rings other than the hexagonal introduce bond angles that deviate from the typical hexagonal angle.

The electron density of states (EDOS) for a-BC_2N, as depicted in Fig. 5, does not exhibit a well-defined band gap. This finding aligns with the experimental band gap of a-BC_2N, measured at 0.11 eV [23], which is too small to be distinctly captured in the EDOS representation. Consequently, we focus on the energy difference between HOMO and LUMO, determining a value of about 0.08 eV. This result is reasonably

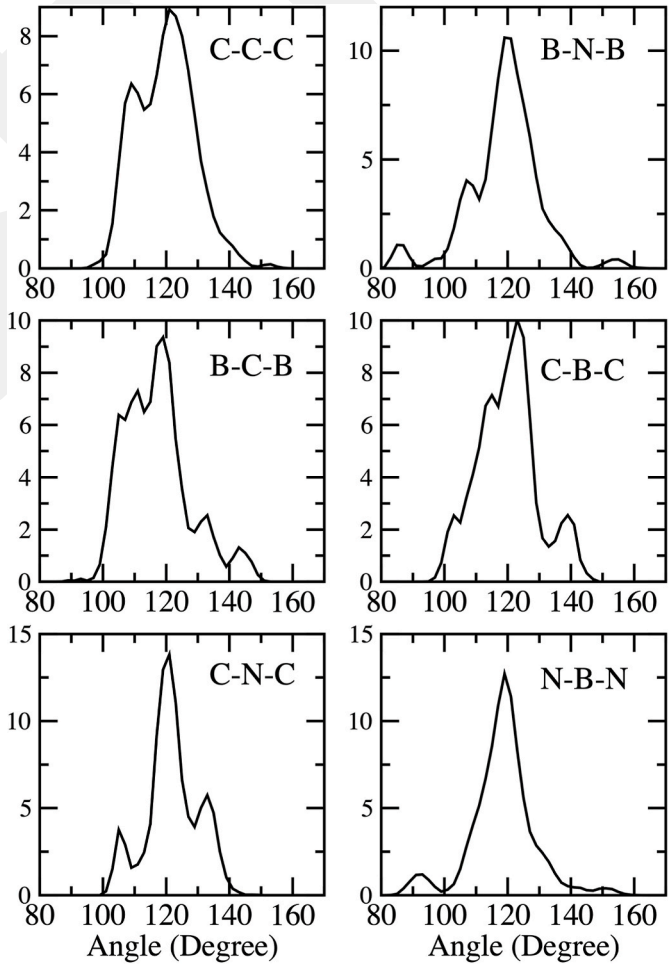

Fig. 3. Bond angle distribution for the amorphous configuration of BC_2N.

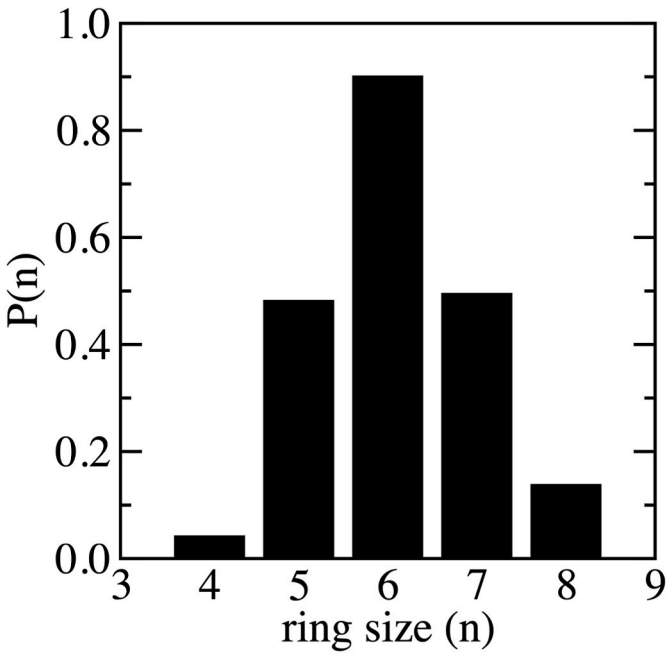

Fig. 4. Ring statistics analysis for a-BC_2N. Here, P(n) indicates the proportion of nodes in the atomic structure that are part of at least one ring of size n.

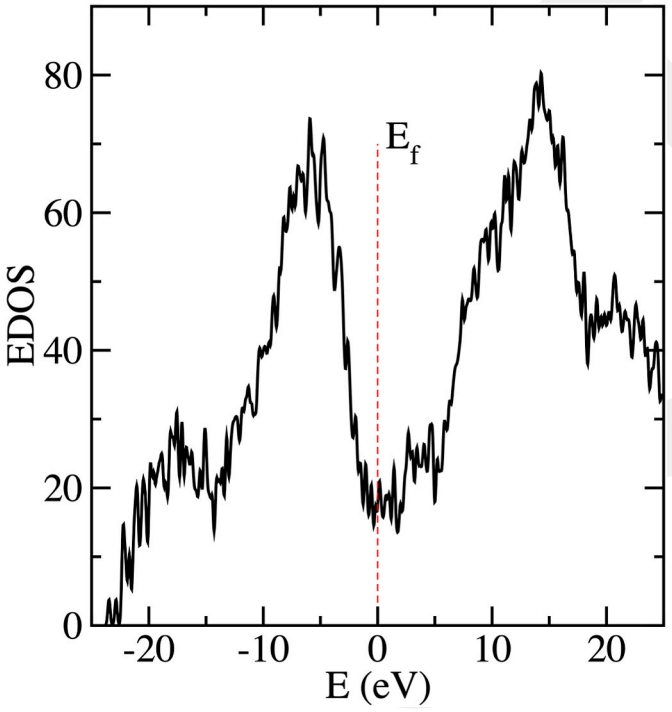

Fig. 5. Electronic density of states (EDOS) for a-BC_2N.

close to the experimental value of 0.11 eV [23], especially considering the known tendency of DFT-GGA to underestimate band gaps. Based on these observations, we propose that a-BC_2N is likely a narrow band gap semiconductor, although uncertainties remain due to inherent approximations within the computational model.

To determine the bulk modulus (K_0) of the model, we examine its energy (E)-volume (V) relationship under hydrostatic pressure, as shown in Fig. 6. Using variable-cell optimization, we obtain comprehensive E-V data, which is then fitted to the third-order Birch-Murnaghan equation of state (EOS). This widely used model describes the relationship

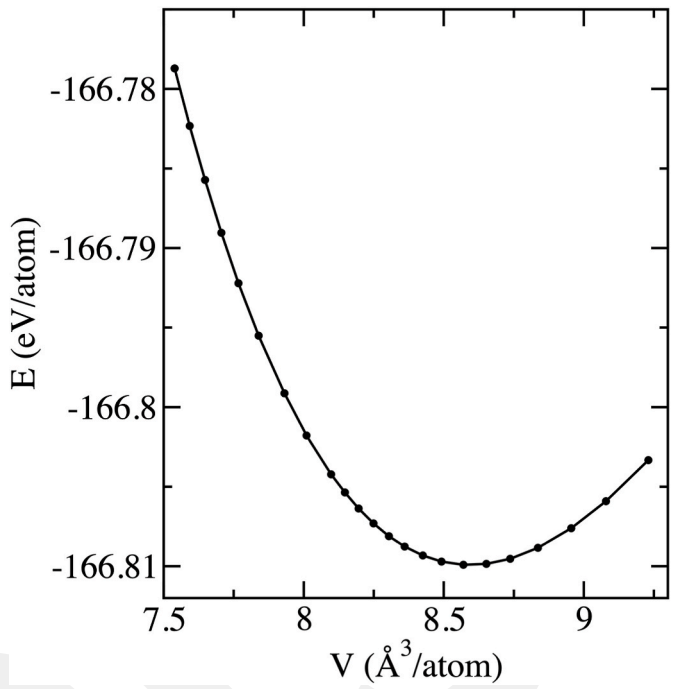

Fig. 6. Energy–volume (E–V) relationship for a-BC_2N, obtained through hydrostatic pressure simulations.

between E, pressure (P), and V in materials under isotropic compression. The energy form of the equation is given as:

$$E(V) = E_0 + \frac{9V_0K_0}{16}\left\{\left[\left(\frac{V_0}{V}\right)^{\frac{2}{3}}-1\right]^3 K_0' + \left[\left(\frac{V_0}{V}\right)^{\frac{2}{3}}-1\right]^2\left[6-4\left(\frac{V_0}{V}\right)^{\frac{2}{3}}\right]\right\}$$

where $E(V)$ is the total energy at a given volume V, E_0 is the energy at equilibrium volume V_0,

K_0 is the bulk modulus zero pressure and K_0' is the pressure derivative of the bulk modulus.

This fitting procedure yields an estimated bulk modulus of 54.4 GPa for a-BC_2N. Table 2 compares this bulk modulus and other mechanical properties of a-BC_2N against reference materials [51–63], showing that a-BC_2N has a considerably higher bulk modulus than many related materials, except a-BC_4N.

To further characterize the mechanical properties of this material, we calculate the Poisson's ratio (ν) by applying uniaxial stress along the diagonal elements of the simulation cell vectors, while simultaneously allowing for relaxation of the remaining stress components. This process involves simultaneous optimization of atomic positions and cell dimensions. The relationship between lateral strain ($\varepsilon_{lateral}$) - applied strain ($\varepsilon_{applied}$), as shown in Fig. 7, is then utilized to derive the Poisson's ratio:

$$\nu = -\frac{\varepsilon_{lateral}}{\varepsilon_{applied}}.$$

By averaging six different values, we obtain a Poisson's ratio of 0.37, surpassing the typical range (0.17–0.28) observed for most related materials but comparable to that of graphite (0.31–0.36).

Young's modulus (E), a crucial measure of stiffness, is subsequently calculated using the following relationship:

$$E = 3K(1-2\upsilon).$$

The resulting value, 42.4 GPa, exceeds the typical range for layered materials (21–32 GPa), indicating enhanced stiffness in a-BC_2N.

To assess shear resistance, the shear modulus (μ) is computed using:

Table 2
Bulk (K), Young (E) and shear (μ) moduli and Poisson ratio (ν). and Vickers hardness (H). The notations 'a,' 'g,' and 'm' respectively denote amorphous, graphite-like, and monolayer structures.

Structure	K (GPa)	E (GPa)	μ (GPa)	ν	H (GPa)	Reference
a-BC_2N	54.4	42.4	15.48	0.37	1.53–2.69	This Study
m-BC_2N	14.63	22.81	9.20	0.24		[51]
a-BC_4N	61.81	28.8	10.12	0.42	0.027–1.53	[52]
g-BC_4N	18.1 ± 0.2					[53]
g-$BC_{2.14}N$	$19.2^{\pm}0.3$					[54]
g-$BC_{1.28}N$	$20.4^{\pm}0.4$					[54]
g-BC	23(2)					[55]
BN	36.7 ± 0.5					[56]
graphite	33.8					[57]
		25.5	9.7	0.31		[58]
	36.3	29.8	10.9	0.36	1.3	[59]
a-graphite	37.9					[60]
		23–32	10–13	0.12–0.15		[61]
					2–3	[62]
a-BC_5	33.9	29.2	10.8	0.35	1.63–1.85	[63]

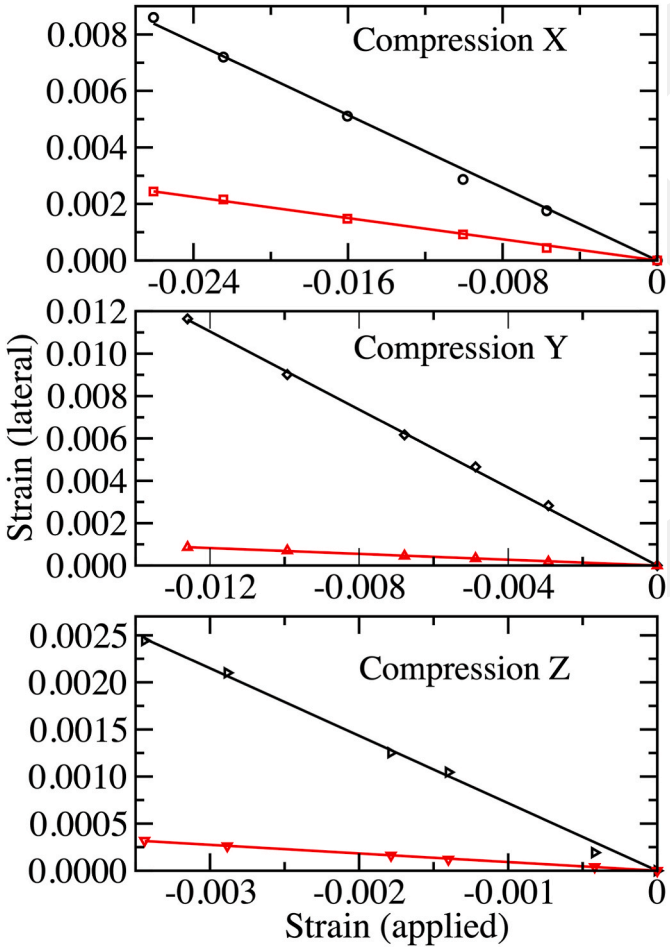

Fig. 7. The relationships between lateral strain ($\varepsilon_{lateral}$) and applied strain ($\varepsilon_{applied}$) for the uniaxial compressions.

$$\mu = \frac{E}{2(1+\nu)}.$$

The estimated shear modulus of 15.4 GPa is consistent with values observed in comparable materials, reflecting moderate resistance to shearing forces.

Finally, we evaluate Vickers hardness (H) using three empirical formulas:

$$H = 0.151\ \mu$$

$$H = 0.92 \left(\frac{1}{n}\right)^{1.137} (\mu)^{0.708}$$

$$H = 0.0635\ E.$$

These formulas estimate Vickers hardness in the range of 1.5–2.7 GPa, consistent with values reported for comparable materials.

4. Discussion

This study provides new insights into the structural, electronic, and mechanical properties of a-BC_2N, contributing to a more comprehensive understanding of BCN compounds. The atomic structure of a-BC_2N, characterized by a layer-like topology and a solid-solution distribution of B, C, and N atoms, represents a significant deviation from the lowest-energy crystalline structure with ordered C–C and B–N layers. In contrast, a-BC_2N displays a random atomic arrangement, resulting in small distinct C-rich and BN-rich domains. This unique feature, previously discussed theoretically for BC_2N systems [1,35], is here confirmed experimentally for the first time in an amorphous structure. Furthermore, the disordered arrangement forms irregular short zigzag chains of C–C and B–N bonds, reminiscent of the zigzag motifs found in stable BC_2N sheet [35]. These zigzag configurations suggest that each layer retains partial structural characteristics of the ordered BC_2N sheet.

The electronic structure analysis reveals that a-BC_2N is likely semiconductor with a HOMO-LUMO gap of approximately 0.08 eV, closely aligning with the experimentally observed value of 0.11 eV. Although this bandgap is narrow, the semiconducting nature of a-BC_2N suggests applications in fields where materials with low electronic bandgaps are advantageous, such as in devices requiring moderate electronic conductivity.

Mechanically, a-BC_2N exhibits a high bulk modulus, indicating high resistance to compression. This robust bulk modulus may stem from

increased interlayer connectivity and the heterogeneous arrangement of B, C, and N atoms within the amorphous structure. However, its Young's modulus and shear modulus suggest moderate stiffness and shear resistance.

While the current 384-atom model offers valuable insights into a-BC_2N, limitations in model size may affect the generalizability of these findings. Specifically, potential size effects could influence observed bonding patterns, the distribution of fourfold coordination motifs, and the formation of C- and BN-rich domains in larger systems. Future studies with larger simulation models or experimental validation are encouraged to confirm these preliminary observations. Such research could elucidate variations in domain size, improve the understanding of structural stability, and provide further insights into local bonding environments, particularly within larger C- and BN-rich clusters. These steps would lead to a more complete understanding of a-BC_2N's potential, paving the way for applications in electronics, flexible materials, and composite systems where both structural resilience and electronic tunability are desirable.

5. Conclusion

In summary, this ab initio study provides the first in-depth analysis of the atomic structure and properties of a- BC_2N. The results indicate that the disordered atomic arrangement of a-BC_2N, with its diverse bonding configurations, forms a solid-solution-like structure rather than the ordered C–C and B–N layers observed in the crystalline form. The electronic structure analysis reveals narrow-band semiconducting behavior, suggesting potential applications in electronics, particularly in devices where low-bandgap materials are advantageous. Mechanically, a-BC_2N exhibits characteristics typical of layered materials but with a higher bulk modulus than many similar structures, indicating enhanced resistance to compression. These distinct structural, electronic, and mechanical properties make a-BC_2N a promising candidate for further research and potential applications.

Declaration of generative AI and AI-assisted technologies in the writing process

During the preparation of this work the author(s) used some AI tools in order to improve the language. After using this tool/service, the author(s) reviewed and edited the content as needed and take(s) full responsibility for the content of the publication.

Declaration of competing interest

The authors declare that they have no known competing financial interests or personal relationships that could have appeared to influence the work reported in this paper.

Acknowledgments

The author extends gratitude to the Abdullah Gül University Support Foundation for their support. The author acknowledges the computing resources and time generously provided by TÜBİTAK ULAKBİM High Performance and Grid Computing Center (TRUBA resources).

Data availability

Data will be made available on request.

References

[1] S. Angizi, M.A. Akbar, M. Darestani-Farahani, P. Kruse, E.C.S.J. Solid, State Sci. Technol. 9 (2020) 083004.
[2] H. Garg, S. Patial, P. Raizada, V.-H. Nguyen, S.Y. Kim, Q.V. Le, T. Ahamad, et al., Chemosphere 313 (2023) 137610.
[3] C.H. Lee, V.K. Kayastha, J. Wang, Y.K. Yap, BCN Nanotubes and Related Nanostructures, 2009, p. 1.
[4] V.L. Solozhenko, S.F. Matar, Materials 16 (2023) 886.
[5] S. Nakano, M. Akaishi, T. Sasaki, S. Yamaoka, Chem. Mater. 6 (1994) 2246.
[6] E. Knittle, R.B. Kaner, R. Jeanloz, M.L. Cohen, Phys. Rev. B 51 (1995) 12149.
[7] T. Komatsu, M. Nomura, Y. Kakudate, S. Fujiwara, J. Mater. Chem. 6 (1996) 1799.
[8] V.L. Solozhenko, D. Andrault, G. Fiquet, M. Mezouar, D.C. Rubie, Appl. Phys. Lett. 78 (2001) 1385.
[9] Y. Zhao, D.W. He, L.L. Daemen, T.D. Shen, R.B. Schwarz, Y. Zhu, D.L. Bish, J. Huang, J. Zhang, G. Shen, J. Qian, T.W. Zerda, J. Mater. Res. 17 (2002) 3139.
[10] H. Sun, S.-H. Jhi, D. Roundy, M.L. Cohen, S.G. Louie, Phys. Rev. B 64 (2001) 094108.
[11] X.F.Z.J. Sun, G.R. Qian, J. Chen, Y.X. Fan, H.T. Wang, X.J. Guo, J.L. He, Z.Y. Liu, Y. J. Tian, Appl. Phys. Lett. 89 (2006) 151911.
[12] X. Luo, X. Guo, B. Xu, Q. Wu, Q. Hu, Z. Liu, J. He, D. Yu, Y. Tian, H. Wang, Phys. Rev. B 76 (2007) 094103.
[13] X. Zhou, J. Sun, Y. Fan, J. Chen, H. Wang, X. Guo, J. He, Y. Tian, Phys. Rev. B 76 (2007) 100101R.
[14] X. Luo, X. Guo, Z. Liu, J. He, D. Yu, B. Xu, Y. Tian, H. Wang, Phys. Rev. B 76 (2007) 092107.
[15] S. Chen, X.G. Gong, S.-H. Wei, Phys. Rev. Lett. 98 (2007) 015502.
[16] C. Chen, H. Sun, Phys. Rev. Lett. 99 (2007) 159601.
[17] S. Chen, X.G. Gong, S.-H. Wei, Phys. Rev. Lett. 99 (2007) 159602.
[18] Q. Li, M. Wang, A.R. Oganov, T. Cui, Y. Ma, G. Zou, J. Appl. Phys. 105 (2009).
[19] X. Wang, Y. Wang, M. Zhang, H. Liu, Phys. Rev. B 107 (2023) 134101.
[20] C.-L. Jiang, W. Zeng, F.-S. Liu, B. Tang, Q.-J. Liu, J. Phys. Chem. Solid. 140 (2020) 109349.
[21] T. Sasaki, M. Akaishi, S. Yamaoka, Y. Fujiki, T. Oikawa, Chem. Mater. 5 (1993) 695.
[22] R. Riedel, J. Bill, G. Passing, Adv. Mater. 3 (1991) 551.
[23] B. Yao, W.J. Chen, L. Liu, B.Z. Ding, W.H. Su, J. Appl. Phys. 84 (1998) 1412.
[24] Q. Wu, Z. Liu, Q. Hu, H. Li, J. He, D. Yu, D. Li, Y. Tian, J. Phys. Condens. Matter 18 (2006) 9519.
[25] C. Popov, K. Saito, B. Ivanov, Y. Koga, S. Fujiwara, V. Shanov, Thin Solid Films 312 (1998) 99.
[26] R. Riedel, J. Bill, G. Passing, Adv. Mater. 3 (1991) 551.
[27] J.P. Nicolich, F. Hofer, G. Brey, R. Riedel, J. Am. Ceram. Soc. 84 (2001) 279.
[28] S. Bhat, S. Lauterbach, D. Dzivenko, C. Lathe, L. Bayarjargal, M. Schwarz, H.-J. Kleebe, E. Kroke, B. Winkler, R. Riedel, J. Phys. Conf. Ser. 500 (2014) 182004.
[29] M.O. Watanabe, S. Itoh, K. Mizushima, T. Sasaki, Appl. Phys. Lett. 68 (1996) 2962.
[30] X.-G. Luo, Z.-Y. Liu, X.-J. Guo, J.-L. He, D.-L. Yu, Y.-J. Tian, J. Sun, H.-T. Wang, Chin. Phys. Lett. 23 (2006) 2175.
[31] S. Azevedo, Eur. Phys. J. B 44 (2005) 203.
[32] M.S.C. Mazzoni, R.W. Nunes, S. Azevedo, H. Chacham, Phys. Rev. 73 (2006) 073108.
[33] P. Saalfrank, W. Rumler, H.U. Hummel, J. Ladik, Synth. Met. 52 (1992) 1.
[34] Z.C. Pan, H. Sun, C.F. Chen, Phys. Rev. B 73 (2006) 193304.
[35] A.Y. Liu, R.M. Wentzcovitch, M.L. Cohen, Phys. Rev. B 39 (1989) 1760.
[36] H. Nozaki, S. Itoh, J. Phys. Chem. Solid. 57 (1996) 41.
[37] J.M. Soler, E. Artacho, J.D. Gale, A. García, J. Junquera, P. Ordejón, D. Sánchez-Portal, J. Phys. Condens. Matter 14 (2002) 2745.
[38] N. Troullier, J.L. Martins, Phys. Rev. B 43 (1991) 1993.
[39] J.P. Perdew, K. Burke, M. Ernzerhof, Phys. Rev. Lett. 77 (1996) 3865.
[40] S. Grimme, J. Comput. Chem. 27 (2006) 1787.
[41] M. Parrinello, A. Rahman, J. Appl. Phys. 52 (1981) 7182.
[42] S. Le Roux, V. Petkov, J. Appl. Crystallogr. 43 (2010) 81.
[43] K. Momma, F. Izumi, J. Appl. Crystallogr. 44 (2011) 1272.
[44] B. Bhattarai, A. Pandey, D.A. Drabold, Carbon 131 (2018) 168.
[45] S.F. Parker, S. Imberti, S.K. Callear, P.W. Albers, Chem. Phys. 427 (2013) 44.
[46] Y. Kumashiro (Ed.), Electric Refractory Materials, Taylor & Francis, New York, 2000.
[47] S. Datta, P. Singh, D. Jana, C.B. Chaudhuri, M.K. Harbola, D.D. Johnson, A. Mookerjee, Carbon 168 (2020) 125.
[48] H. Lu, Y. Guo, J.W. Martin, M. Kraft, J. Robertson, Carbon 147 (2019) 483.
[49] Q. Hu, Q. Wu, Y. Ma, L. Zhang, Z. Liu, J. He, H. Sun, H.T. Wang, Y. Tian, Phys. Rev. B 73 (2006) 214116.
[50] D. Tomanek, R.M. Wentzcovitch, S.G. Louie, M.L. Cohen, Phys. Rev. B 37 (1988) 3134.
[51] A. Bafekry, M. Naseri, M. Faraji, M.M. Fadlallah, D.M. Hoat, H.R. Jappor, M. Ghergherehchi, D. Gogova, H. Afarideh, Sci. Rep. 12 (2022) 22269.
[52] M. Durandurdu, J. Non-Cryst. Solids 639 (2024) 123090.
[53] V.L. Solozhenko, V.Z. Turkevich, T. Sato, J. Am. Ceram. Soc. 80 (1997) 3229.
[54] V.L. Solozhenko, Eur. J. Solid State Inorg. Chem. 34 (1997) 797.
[55] V.L. Solozhenko, O.O. Kurakevych, E.G. Solozhenko, J. Chen, J.B. Parise, Solid State Commun. 137 (2006) 268.
[56] V.L. Solozhenko, G. Will, F. Elf, Solid State Commun. 96 (1995) 1.
[57] M. Hanfland, H. Beister, K. Syassen, Phys. Rev. B 39 (1989) 12598.
[58] J.R. Cost, K.R. Janowski, R.C. Rossi, Philos. Mag. A 17 (1968) 851.
[59] K. Luo, B. Liu, L. Sun, Z. Zhao, Y. Tian, Chin. Phys. Lett. 38 (2021) 028102.
[60] X. Wang, Z.X. Bao, Y.L. Zhang, F.Y. Li, R.C. Yu, C.Q. Jin, J. Appl. Phys. 93 (2003) 1991.
[61] J.X. Zhao, R.C. Bradt, P.L. Walker Jr., Carbon 23 (1985) 15.
[62] J. Robertson, J. Non-Cryst. Solids 137 (1991) 825.
[63] M. Durandurdu, J. Non-Cryst. Solids 592 (2022) 121743.